

Correlating uncertainties in global analyses within SMEFT matters

Stefan Bissmann,^{*} Johannes Erdmann,[†] Cornelius

Grunwald,[‡] Gudrun Hiller,[§] and Kevin Kröninger[¶]

Fakultät Physik, TU Dortmund, Otto-Hahn-Str.4, D-44221 Dortmund, Germany

We investigate the impact of correlations between (theoretical and experimental) uncertainties on multi-experiment, multi-observable analyses within the Standard Model Effective Field Theory (SMEFT). To do so, we perform a model-independent analysis of t -channel single top-quark production and top-quark decay data from ATLAS, CMS, CDF and D0. We show quantitatively how the fit changes when different experimental or theoretical correlations are assumed. Scaling down statistical uncertainties according to the luminosities of future colliders with 300 fb^{-1} and higher, we find that this effect becomes a matter of life and death: assuming no correlations returns a fit in agreement with the Standard Model while a 'best guess'-ansatz taking into account correlations would observe new physics. At the same time, modelling the impact of higher order SMEFT-corrections the latter turn out to be a subleading source of uncertainty only.

I. INTRODUCTION

The Standard Model Effective Field Theory (SMEFT) allows for model-independent analyses of multi-experiment, multi-observable data [1–3]. Higher-dimensional operators, built from Standard Model (SM) fields consistent with $SU(3)_C \times SU(2)_L \times U(1)_Y$ - and Lorentz-invariance, systematically account for physics beyond the SM (BSM) at the scale Λ above the electroweak one, in an expansion in $1/\Lambda$. Along the lines of high luminosity precision programs in flavor physics [4], new physics at scales beyond the colliders energy reach is probed indirectly, making global fits and uncertainty management key tasks.

Correlations between measurements play an important role in global fits, e.g., recently discussed in [5–7]. However, the quantitative impact of such correlations continues to be unknown. In practice, this has led to simplifying assumptions as well as the exclusion of data sets from global

^{*}Electronic address: stefan.bissmann@tu-dortmund.de

[†]Electronic address: johannes.erdmann@tu-dortmund.de

[‡]Electronic address: cornelius.grunwald@tu-dortmund.de

[§]Electronic address: ghiller@physik.uni-dortmund.de

[¶]Electronic address: kevin.kroeninger@tu-dortmund.de

fits. A first toy study of correlations has been discussed in Ref. [8].

In this paper, we work out how correlations of systematic uncertainties and theory uncertainties between measurements change fit results within the SMEFT framework. We entertain the example of t -channel single top-quark production together with top-quark decay; it is rather compact due to the small number of contributing Wilson coefficients, while still covers all relevant aspects of a global fit with various observables from different experiments. In the recent past, several studies of the top-quark sector of SMEFT have been performed, see, for instance, Refs. [5–21].

This paper is organized as follows. In Sec. II we introduce the SMEFT framework and effective couplings relevant to our analysis and describe the computations of SM and BSM contributions to single top-quark production and top-quark decays. In Sec. III we discuss the methodology of our analysis and the experimental input. We consider different scenarios for correlations between measurements and demonstrate how such correlations affect the results of fits to current data. Furthermore we study the impact of correlations for future high-luminosity experiments. In Sec. IV we conclude.

II. SMEFT APPROACH TO TOP-QUARK PHYSICS

The SMEFT Lagrangian \mathcal{L}_{eff} is organized as an expansion in powers of Λ^{-1} . Higher dimensional operators $O_i^{(d)}$ of dimension d are added to the SM Lagrangian \mathcal{L}_{SM} together with a corresponding Wilson coefficient $C_i^{(d)}$ and a factor Λ^{d-4} . Since we assume that a gap exist between the scale of new physics and the electroweak scale, we keep only the leading contributions at $\mathcal{O}(\Lambda^{-2})$:

$$\mathcal{L}_{\text{eff}} = \mathcal{L}_{\text{SM}} + \sum_i \frac{C_i^{(6)}}{\Lambda^2} O_i^{(6)} + \mathcal{O}(\Lambda^{-4}) . \quad (1)$$

In the following we study t -channel single top-quark production cross sections and top-quark decay observables. The following operators contribute at $\mathcal{O}(\Lambda^{-2})$:

$$\begin{aligned} O_{\phi q}^{(3)} &= i \left(\phi^\dagger \overleftrightarrow{D}_\mu^I \phi \right) (\bar{q}_L \gamma^\mu \tau^I q_L) , & O_{tW} &= (\bar{q}_L \sigma^{\mu\nu} \tau^I t_R) \tilde{\phi} W_{\mu\nu}^I , \\ O_{qq}^{(1)} &= (\bar{q}_L \gamma_\mu q_L) (\bar{q}_L \gamma^\mu q_L) , & O_{qq}^{(3)} &= (\bar{q}_L \gamma_\mu \tau^I q_L) (\bar{q}_L \gamma^\mu \tau^I q_L) , \end{aligned} \quad (2)$$

where ϕ denotes the Higgs field, $\tilde{\phi}_i = \epsilon_{ij} \phi_j^*$ ($\epsilon_{12} = 1$), q_L is the $SU(2)$ doublet, t_R the top-quark $SU(2)$ singlet and $W_{\mu\nu}^I$ and τ^I are the field strength tensor and the generators of $SU(2)_L$, respectively. Neglecting contributions proportional to masses $m \ll m_t$, where m_t is the top-quark mass, the observables depend on three coefficients:

$$\tilde{C}_{\phi q}^{(3)} , \quad \tilde{C}_{tW} , \quad \tilde{C}_{qq} = \tilde{C}_{qq}^{(3)1133} + \frac{1}{6} \left(\tilde{C}_{qq}^{(1)1331} - \tilde{C}_{qq}^{(3)1331} \right) , \quad (3)$$

with $\tilde{C}_i = C_i v^2 / \Lambda^2$ and the Higgs vacuum expectation value $v = 246$ GeV. The additional indices denote the quark generation of the $SU(2)_L$ doublets in $O_{qq}^{(1)}$ and $O_{qq}^{(3)}$.

In Sec. II A and Sec. II B we discuss single top-quark production and top-quark decay, respectively.

A. t -channel single top-quark production

We employ the Monte Carlo generator `MadGraph5` [22] and the `dim6top_LO` UFO model [21] to compute SM and BSM contributions to total and differential cross sections of t -channel single top-quark production at parton level at leading order. We validate our results with `PYTHIA 8` [23, 24] and find good agreement. For all computations we utilize the MSTW20008lo [25] parton distribution function (PDF) set. To reduce the impact of higher order QCD corrections we take into account SM cross sections at NLO. For differential cross sections we apply k -factors to the SM predictions using the NLO predictions presented in the experimental analyses in Refs. [26–29]. We validate the results by computing the observables at NLO applying `MadGraph5` with different PDF sets: MSTW20008nlo [25], CT10nlo [30], NNPDF23_nlo [31]. We find good agreement for all three PDF sets. Total cross sections are computed at NLO using `MadGraph5` with the same PDF sets. Renormalization and factorization scales are set to $\mu_{R,F} = m_t$ with $m_t = 172.8$ GeV. Scale uncertainties are evaluated by varying renormalization and factorization scales independently between $m_t/2 \leq \mu_{R,F} \leq 2m_t$. We take the maximal variation as the uncertainty. We compute PDF uncertainties with `MadGraph5` using the same PDF sets. We take the central value as the estimate and the total 1σ range, for which we add statistical, PDF uncertainties and scale variation uncertainties in quadrature, as the theory uncertainty.

B. Top-quark decay

The decay width Γ_t of the top quark and the W boson helicity fractions F_i are measured by extracting $t\bar{t}$ events in the lepton+jets channel with $t \rightarrow Wb$. Hence, we consider only operators modifying the Wtb vertex in Eq. (2), O_{tW} and $O_{\phi q}^{(3)}$. Contributions from other dimension-six operators are proportional to the mass of the bottom quark m_b , and hence neglected. We include BSM contributions at LO and the SM ones at NNLO [32, 33].

III. STUDYING THE IMPACT OF CORRELATIONS

We employ EFT *fitter* [34] to determine constraints on the Wilson coefficients using a Bayesian ansatz. We include data from ATLAS [26, 27, 35–38], CMS [28, 29, 39–44], CDF and D0 [45–47], given in Tab. I.

Process	\sqrt{s}	Luminosity	Experiment	Observable	Reference
Single top	7 TeV	4.59 fb ⁻¹	ATLAS	$\sigma(tq), \sigma(\bar{t}q), d\sigma(tq)/dp_T, d\sigma(\bar{t}q)/dp_T$	[26]
		1.17 fb ⁻¹ (μ)	CMS	$\sigma(tq + \bar{t}q)$	[39]
		1.56 fb ⁻¹ (e)	CMS	$\sigma(tq + \bar{t}q)$	[39]
Single top	8 TeV	20.2 fb ⁻¹	ATLAS	$\sigma(tq), \sigma(\bar{t}q), d\sigma(tq)/dp_T, d\sigma(\bar{t}q)/dp_T$	[27]
		19.7 fb ⁻¹	CMS	$\sigma(tq), \sigma(\bar{t}q), \sigma(tq + \bar{t}q), d\sigma/d y(t/\bar{t}) $	[28, 40]
Single top	13 TeV	3.2 fb ⁻¹	ATLAS	$\sigma(tq), \sigma(\bar{t}q)$	[35]
		2.2 fb ⁻¹	CMS	$\sigma(tq), \sigma(\bar{t}q), \sigma(tq + \bar{t}q)$	[41]
		2.3 fb ⁻¹	CMS	$d\sigma/d y(t/\bar{t}) $	[29]
Top decay	1.96 TeV	2.7 fb ⁻¹	CDF	F_0	[45]
		8.7 fb ⁻¹	CDF	F_0	[46]
		5.4 fb ⁻¹	D0	F_0	[47]
Top decay	7 TeV	1.04 fb ⁻¹	ATLAS	F_0, F_L	[37]
		5.0 fb ⁻¹	CMS	F_0, F_L	[42]
Top decay	8 TeV	20.2 fb ⁻¹	ATLAS	Γ_t	[36]
		20.2 fb ⁻¹	ATLAS	F_0, F_L	[38]
		19.7 fb ⁻¹	CMS	F_0, F_L	[43]
Top decay	13 TeV	19.8 fb ⁻¹	CMS	F_0, F_L	[44]

TABLE I: The experimental measurements of top-quark production and decay considered in this analysis. For both processes we indicate the center of mass energy \sqrt{s} , the integrated luminosity, the experiment, the observables included in the analysis and the publication reference.

We count each bin of differential distributions as one observable and include in total 55 measurements of 41 different observables. If differential cross sections are presented in terms of normalized distributions, we reconstruct absolute distributions using total cross sections. We take a constant prior for the parameter interval $-1 \leq \tilde{C}_i \leq 1$ as default.

We consider both a linear and quadratic fit ansatz for the observables. For the example of total

cross sections, the linear one reads

$$\sigma = \sigma_{\text{SM}} + \sum_i \tilde{C}_i \sigma_i, \quad (\text{'linear'}), \quad (4)$$

where σ_{SM} denotes the SM contribution and σ_i are the LO interference terms at $\mathcal{O}(1/\Lambda^2)$ between SM and BSM. Specifically, in the linear ansatz, the quadratic BSM terms following from squaring amplitudes linear in the Wilson coefficients, are omitted, as they are formally of higher order, $\mathcal{O}(\Lambda^{-4})$, even though they are induced by dimension six operators.

The quadratic ansatz reads

$$\sigma = \sigma_{\text{SM}} + \sum_i \tilde{C}_i \sigma_i + \sum_{i \leq j} \tilde{C}_i \tilde{C}_j \sigma_{ij}, \quad (\text{'quadratic'}), \quad (5)$$

where the purely BSM contributions from dimension six operators σ_{ij} contributing at $\mathcal{O}(1/\Lambda^4)$ are kept. To study the performance of the SMEFT-fit in view of the power corrections v^2/Λ^2 , we compare results in the linear, the quadratic approximation and in a third EFT-implementation ('linear+ δ_{EFT} ') based on the linear ansatz where we add an additional relative systematic theory uncertainty $\delta_{\text{EFT}} \sim v^2/(1 \text{ TeV})^2$ to each observable to model higher order effects.

In Sec. III A we provide our set-up for correlated uncertainties. Fit results for present and hypothetical future data are presented in Sec. III B and Sec. III C, respectively. In Sec. III D we compare our findings assuming no correlations to results in the literature.

A. Uncertainty set-ups

We consider three different types of uncertainties: Statistical uncertainties, systematic uncertainties and theory uncertainties. In the statistical analysis with *EFTfitter* the uncertainties of all measurements are assumed to be Gaussian distributed. As described in Ref. [34], correlations are taken into account for all types of uncertainties (here: statistical, systematic and theory) by calculating the total covariance matrix \mathcal{M} as the sum of the individual covariance matrices $\text{cov}^{(k)}[x_i, x_j]$

$$\mathcal{M}_{ij} = \text{cov}[x_i, x_j] = \sum_k \text{cov}^{(k)}[x_i, x_j] = \sum_k \rho_{ij}^{(k)} \sigma_i^{(k)} \sigma_j^{(k)}, \quad (6)$$

where x_i denotes the measurements, $\sigma_i^{(k)}$ are the uncertainty values and $\rho_{ij}^{(k)}$ are the correlation coefficients and the sum is over all types of uncertainties. Correlated statistical uncertainties arise if different observables are extracted from the same data set. Corresponding correlation matrices are mostly known from the experimental analyses [26, 27, 37, 38, 43, 44], and included in our

analysis. In contrast, almost no information about the correlation of systematic uncertainties or theory uncertainties is provided. To study their impact on the results of the fit we choose a simple parametrization of the correlation matrices. In the case of systematic uncertainties, correlations between measurements by the same experiment at the same energy are set to ρ_{sys} , since such systematic uncertainties are expected to have the same source. Moreover, we expect the uncertainties of observables measured by the same experiment at different energies to be correlated less, and therefore set these entries to $\rho_{\text{sys}}/2$. In contrast, theory uncertainties are not expected to depend on the experiment, but on the energy of the process. Therefore, correlations between measurements at the same energy are set to ρ_{th} . Observables measured at different energies are assumed to be correlated with a coefficient $\rho_{\text{th}}/2$. In the fit with the linear+ δ_{EFT} ansatz correlations between observables of the same process are set to $\rho_{\text{EFT}} = 0.9$. In the linear (4) and quadratic (5) ansatz these correlations are omitted together with the corresponding uncertainties.

It should be noted that F_0 and F_L are always anti-correlated in our set-up since they are required to add up to $1 - F_R$. In the SM, $F_R = 0 + \mathcal{O}(m_b^2/m_t^2)$ due to the $V - A$ structure of the weak interaction. Contributions from O_{tW} are suppressed by a factor m_b^2/m_t^2 and contributions from additional dimension-six operators including right-handed bottom quarks are suppressed by a factor m_b/m_t . We neglect these contributions in the fit.

In the following analysis we demonstrate the impact of the correlation parameters on the fit results by varying ρ_{sys} and ρ_{th} independently within the interval $[0, 1]$, since positive values for the correlations are expected. We also explored the possibility of negative values but found that in this case the covariance matrix is no longer positive semi-definite. We present results for two benchmark scenarios: The 'no correlation' scenario, which has been adopted in previous studies [5, 19, 20], where we neglect all unknown correlations

$$\rho_{\text{sys}} = \rho_{\text{th}} = 0, \quad (\text{'no correlation'}) \quad (7)$$

and the 'best guess' scenario with strong correlations [48]

$$\rho_{\text{sys}} = 0.9, \quad \rho_{\text{th}} = 0.9, \quad (\text{'best guess'}). \quad (8)$$

The correlation matrices for the data given in Tab. I are 55×55 dimensional and too large to be given here explicitly. Instead, we illustrate our parametrization with a simplified one. Suppose a dataset with five measurements: the total cross sections of single top-quark production $\sigma(tq)_7^A$ and single antitop-quark production $\sigma(\bar{t}q)_7^A$ performed by ATLAS at 7 TeV, the total cross section $\sigma(tq)_8^A$ and $\sigma(tq)_8^C$ measured at 8 TeV by ATLAS and CMS, respectively, and the top-quark decay

width Γ_t . In this example, our parametrization of the correlation matrix of systematic uncertainties reads

$$\begin{array}{c} \sigma(tq)_7^A \quad \sigma(\bar{t}q)_7^A \quad \sigma(tq)_8^A \quad \sigma(tq)_8^C \quad \Gamma_t \\ \sigma(tq)_7^A \left(\begin{array}{ccccc} 1 & \rho_{\text{sys}} & \frac{\rho_{\text{sys}}}{2} & 0 & 0 \\ \rho_{\text{sys}} & 1 & \frac{\rho_{\text{sys}}}{2} & 0 & 0 \\ \frac{\rho_{\text{sys}}}{2} & \frac{\rho_{\text{sys}}}{2} & 1 & 0 & 0 \\ 0 & 0 & 0 & 1 & 0 \\ 0 & 0 & 0 & 0 & 1 \end{array} \right), \end{array} \quad (9)$$

while the one of theory uncertainties is written as

$$\begin{array}{c} \sigma(tq)_7^A \quad \sigma(\bar{t}q)_7^A \quad \sigma(tq)_8^A \quad \sigma(tq)_8^C \quad \Gamma_t \\ \sigma(tq)_7^A \left(\begin{array}{ccccc} 1 & \rho_{\text{th}} & \frac{\rho_{\text{th}}}{2} & \frac{\rho_{\text{th}}}{2} & 0 \\ \rho_{\text{th}} & 1 & \frac{\rho_{\text{th}}}{2} & \frac{\rho_{\text{th}}}{2} & 0 \\ \frac{\rho_{\text{th}}}{2} & \frac{\rho_{\text{th}}}{2} & 1 & \rho_{\text{th}} & 0 \\ \frac{\rho_{\text{th}}}{2} & \frac{\rho_{\text{th}}}{2} & \rho_{\text{th}} & 1 & 0 \\ 0 & 0 & 0 & 0 & 1 \end{array} \right). \end{array} \quad (10)$$

The additional matrix of the δ_{EFT} uncertainties included in the linear+ δ_{EFT} ansatz reads

$$\begin{array}{c} \sigma(tq)_7^A \quad \sigma(\bar{t}q)_7^A \quad \sigma(tq)_8^A \quad \sigma(tq)_8^C \quad \Gamma_t \\ \sigma(tq)_7^A \left(\begin{array}{ccccc} 1 & \rho_{\text{EFT}} & \rho_{\text{EFT}} & \rho_{\text{EFT}} & 0 \\ \rho_{\text{EFT}} & 1 & \rho_{\text{EFT}} & \rho_{\text{EFT}} & 0 \\ \rho_{\text{EFT}} & \rho_{\text{EFT}} & 1 & \rho_{\text{EFT}} & 0 \\ \rho_{\text{EFT}} & \rho_{\text{EFT}} & \rho_{\text{EFT}} & 1 & 0 \\ 0 & 0 & 0 & 0 & 1 \end{array} \right), \end{array} \quad (11)$$

with $\rho_{\text{EFT}} = 0.9$ in both the 'no correlation' and 'best guess' scenario.

B. Fit to data

We present results from fits to the data given in Tab. I. The fit is performed with a linear ansatz (4) with and without the additional uncertainty δ_{EFT} , and with a quadratic one (5). In the following we denote with 'central value' the global mode of the posterior distribution. In Fig. 1

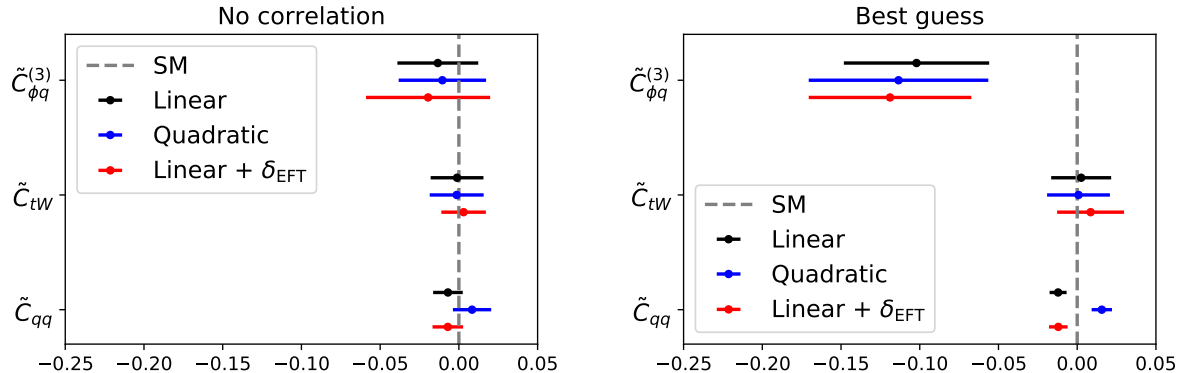


FIG. 1: Marginal constraints on the coefficients \tilde{C}_i from fits with the 'no correlation' scenario (left), Eq. (7), and the 'best guess' scenario (right), Eq. (8). Dots and lines denote the central value and the smallest 95 % interval, respectively, in the 1D projection. The SM is indicated by the vertical dashed line.

we give marginal constraints on each coefficient in the 'no correlation' scenario (left) and the 'best guess' scenario (right). For each coefficient we give the central value (dot) and the smallest 95 % intervals (lines) in the 1D projections. Concerning the different EFT-implementations we find good agreement for $\tilde{C}_{\phi q}^{(3)}$ and \tilde{C}_{tW} . For \tilde{C}_{qq} we find differences between the linear and quadratic models. This can be understood as an effect of the differential cross section data which favor positive shifts relative to the SM prediction. Since the interference terms have a negative sign, negative values of \tilde{C}_{qq} are favored in the linear model while positive values are favored in the quadratic model due to the \tilde{C}_{qq}^2 terms, which are always positive.

Correlations have a significant impact on the results of the fit. While the results for \tilde{C}_{tW} are only slightly affected, we find changes in the 'best guess' scenario compared to the 'no correlation' scenario for both $\tilde{C}_{\phi q}^{(3)}$ and \tilde{C}_{qq} . In the case of \tilde{C}_{qq} the 95 % interval shrinks by a factor of up to 2 while the central value also changes by a factor of up to 1.8, resulting in deviations of up to 4.5σ . Similarly, the central value of $\tilde{C}_{\phi q}^{(3)}$ is shifted away from the SM and the 95 % interval grows by a factor of 2. This gives rise to deviations from the SM of up to 4.4σ .

To detail the impact of systematic and theory uncertainties on the constraints we perform fits in which we vary ρ_{sys} and ρ_{th} independently. In Fig. 2 we give the central value of $\tilde{C}_{\phi q}^{(3)}$ for $\rho_{\text{sys}}, \rho_{\text{th}} = 0.0, 0.3, 0.6, 0.9$ in the different EFT-implementations. The upper-left corner corresponds to the 'no correlation' scenario and the lower-right corner to the 'best guess' scenario. The 95 % region changes with varying correlation coefficients by a factor of up to 1.4 (2.3) in the linear (quadratic/linear+ δ_{EFT}) implementation and is not shown for simplicity. In all three EFT-implementations

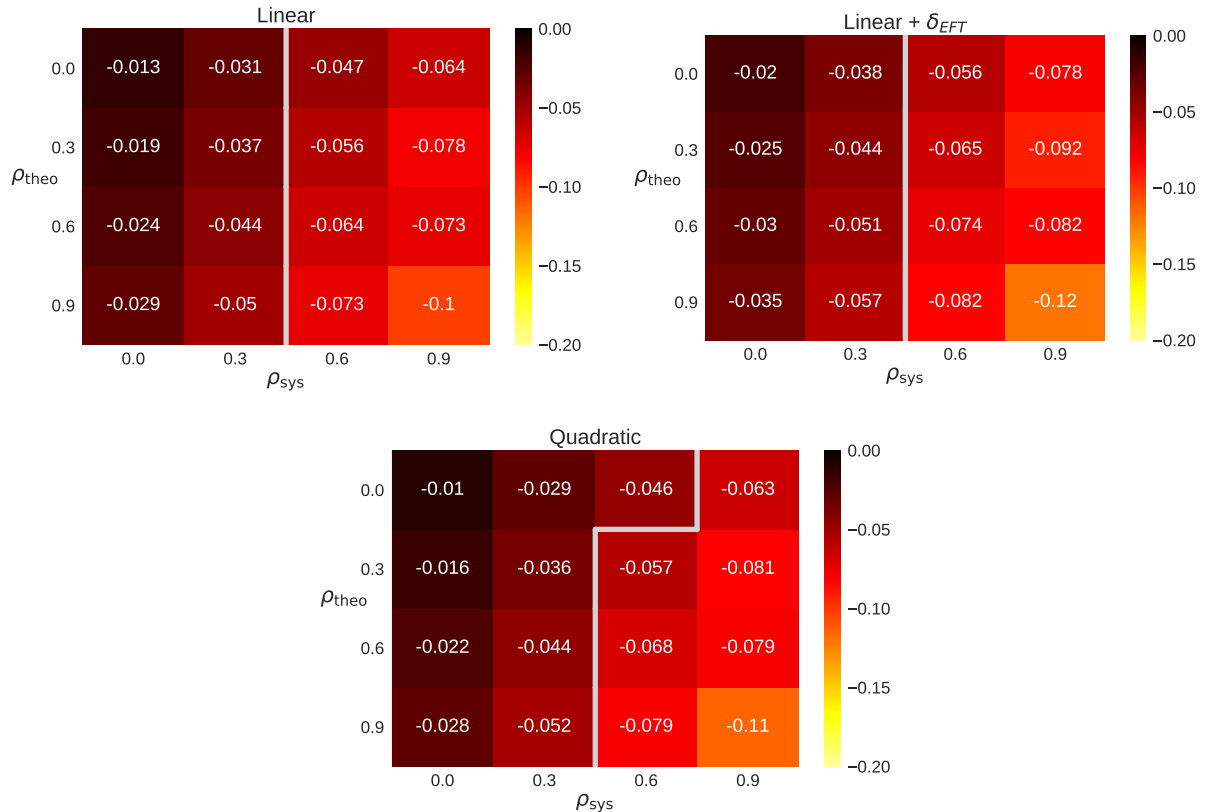


FIG. 2: Central values of $\tilde{C}_{\phi q}^{(3)}$ in the different EFT-implementations for correlation parameters $\rho_{\text{sys}}, \rho_{\text{th}} = 0.0, 0.3, 0.6, 0.9$ from a marginalized fit to the data given in Tab. I. Both correlation parameters are varied independently from each other. The upper-left and lower-right corner correspond to the 'no correlation' scenario in Eq. (7) and the 'best guess' scenario in Eq. (8), respectively. Central values below and to the right of the grey line are in conflict with the SM at more than 2σ .

of the BSM contributions we find very similar results. Correlations of theory uncertainties and systematic uncertainties affect the constraints in a similar way. With increasing values of ρ_i the central value is shifted further away from both the SM and the 'no correlation' scenario. The grey line shows which central values deviate strongly from the 'no correlation' scenario: values below and to the right of the line deviate from the SM by more than 2σ . We find that correlations of systematic uncertainties have a stronger impact on the constraints than correlations of theory uncertainties since even in the case $\rho_{\text{th}} = 0$ we can still find deviations of more than 2σ from the SM while we do not find such deviations for $\rho_{\text{sys}} = 0$.

Correlations affect constraints on \tilde{C}_{qq} and on $\tilde{C}_{\phi q}^{(3)}$, while \tilde{C}_{tW} remains almost unchanged. This is due to the different datasets driving the constraints: \tilde{C}_{tW} is strongly constrained by the helicity

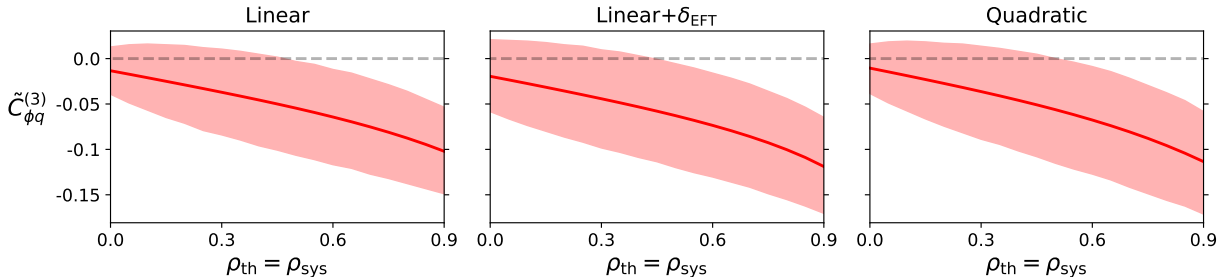


FIG. 3: Central values (red line) and 95 % intervals (red band) of $\tilde{C}_{\phi q}^{(3)}$ in the different EFT-implementations for correlation parameters $\rho_{\text{sys}} = \rho_{\text{th}} \in [0, 0.9]$ from a marginalized fit to the data given in Tab. I.

fractions, which have weaker correlations among each other and smaller uncertainties than single top production data. In contrast, \tilde{C}_{qq} and $\tilde{C}_{\phi q}^{(3)}$ are constrained by the differential and total cross sections. These datasets can be strongly correlated, such that the corresponding constraints on the Wilson coefficients can change significantly with the correlation set-up.

In Fig. 3 we give central values (red line) and the corresponding 95 % intervals (red band) of $\tilde{C}_{\phi q}^{(3)}$ in the different EFT-implementations for correlation parameters $\rho_{\text{sys}} = \rho_{\text{th}} \in [0, 0.9]$ from a marginalized fit to the data given in Tab. I. We find a continuous and consistent behavior of the constraints for increasing correlation parameters. As evident from all Figs. 1-3, stronger correlations result in stronger deviations from the SM.

To validate the stability of our fit, we vary the non-zero off-diagonal entries in the 'best guess' correlation matrices of systematic and theory uncertainties by adding uniformly distributed random numbers $u \in [-0.05, 0.05]$ to the entries. Each element is varied individually while keeping the correlation matrices symmetric. Using the randomized correlation matrices, we perform 3000 marginalized fits to the data given in Tab. I. In Fig. 4 we give histograms for the central value (left) and for the size of the 95 % interval (right) of $\tilde{C}_{\phi q}^{(3)}$ in the linear EFT-implementations for correlation parameters varied randomly around the 'best guess' scenario (8). The black lines denote the results from the 'best guess' scenario. Compared to the 'best guess' scenario, the distribution of the central values is shifted toward more negative values and is slightly asymmetric, favoring values further away from the SM. The distribution of the size of the 95 % interval is shifted to smaller values and shows an asymmetry, favoring smaller intervals. As in Fig. 3, we observe a smooth and stable dependence on the correlation parameters. Similar results are obtained for the quadratic and linear+ δ_{EFT} EFT-implementations (not shown).

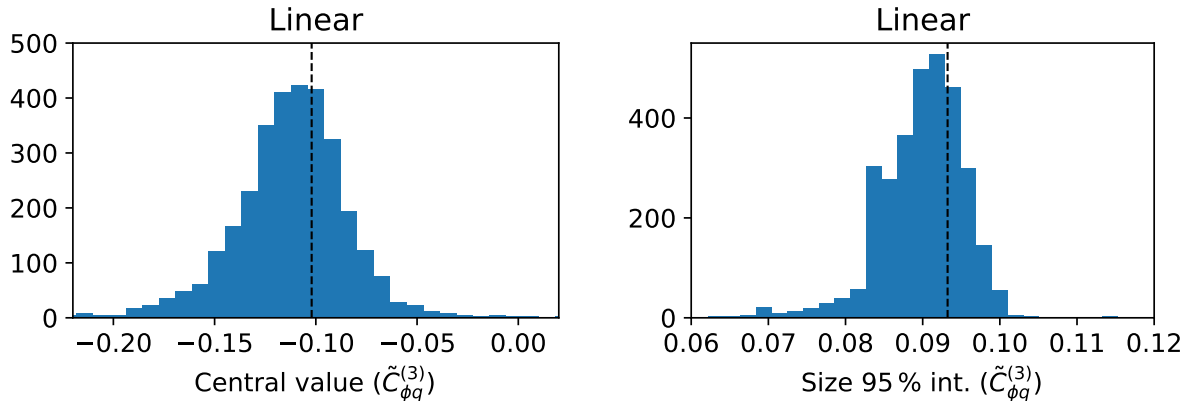


FIG. 4: Histograms of the central value (left) and the size of the 95 % interval (right) of $\tilde{C}_{\phi q}^{(3)}$ in the linear EFT-implementations for correlation parameters varied randomly around the 'best guess' scenario from a marginalized fit to data given in Tab. I. Black lines denote results from the 'best guess' scenario in Eq. (8).

C. Future scenarios

We demonstrate the impact of correlations of systematic and theory uncertainties in the light of the higher integrated luminosity at future experiments, such as LHC Run-3 and HL-LHC [49], considering different future scenarios: 300 fb^{-1} and 3000 fb^{-1} . To do so, we scale statistical uncertainties of the data in Tab. I according to the presumed integrated luminosity keeping the present central values and systematic and theory uncertainties. In Figs. 5 we give marginal constraints for

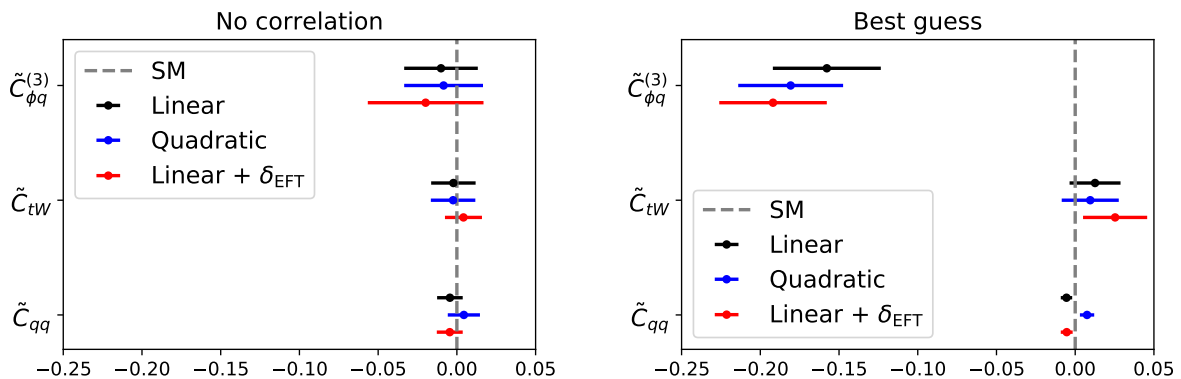


FIG. 5: Same as Fig. 1, but with statistical uncertainties of the data in Tab. I scaled to 300 fb^{-1} , assuming present central values, systematic uncertainties and theory uncertainties.

the coefficients \tilde{C}_i obtained in the 'no correlation' (left) and 'best guess' (right) scenario from fits

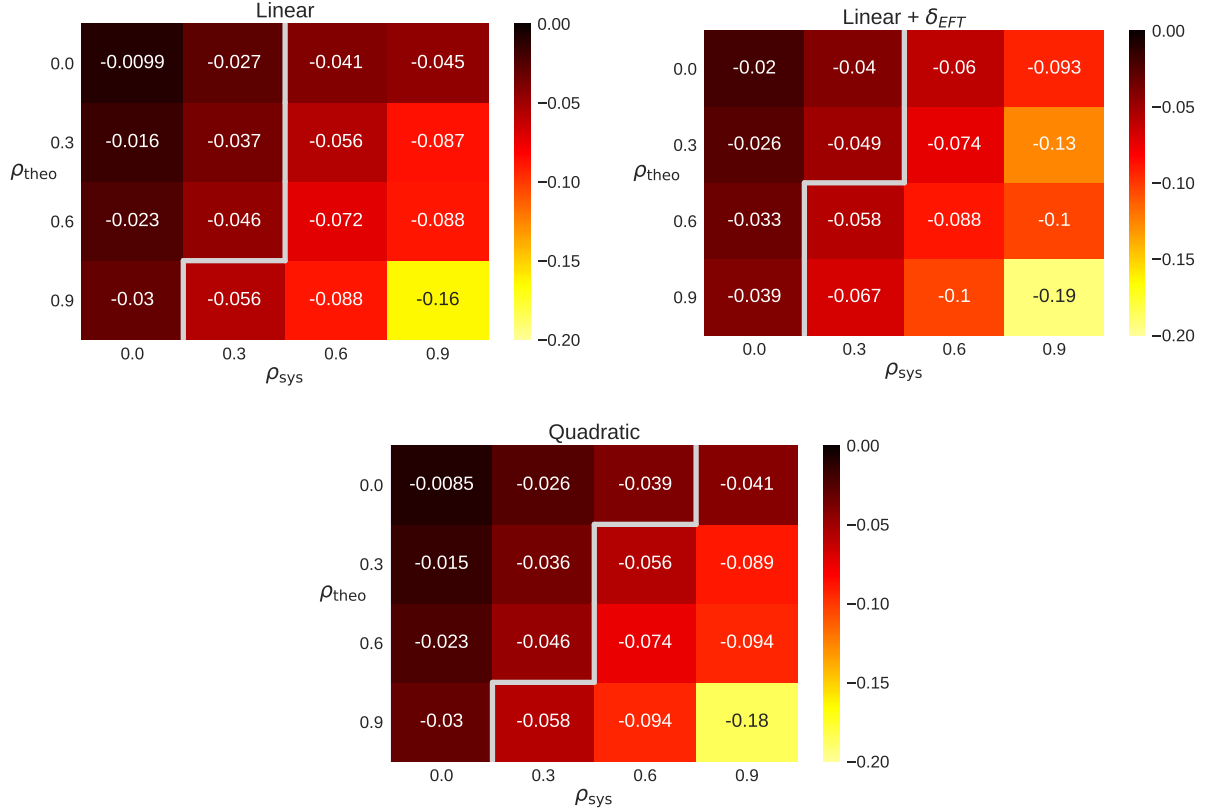


FIG. 6: Same as Fig. 2, but with all statistical uncertainties of the data in Tab. I scaled to the expected integrated luminosity of 300 fb^{-1} , assuming present central values, systematic uncertainties and theory uncertainties.

to data in Tab. I with statistical uncertainties scaled to 300 fb^{-1} . Dots and lines denote the central value and the smallest 95 % interval, respectively. We find that increasing the luminosity from up to 20 fb^{-1} for the data in Tab. I to 300 fb^{-1} improves the constraints on the coefficients in both correlation scenarios.

In contrast, increasing the luminosity further to 3000 fb^{-1} barely improves the constraints (not shown) due to the dominating systematic and theory uncertainties: In the 'no correlation' scenario results for 300 fb^{-1} and 3000 fb^{-1} are the same up to percent level for all coefficients. In the 'best guess' scenario the results change by up to 5 % for $\tilde{C}_{\phi q}^{(3)}$ up to 25 % for \tilde{C}_{tW} and \tilde{C}_{qq} . The constraints in the light of higher luminosity depend strongly on the correlation scenario: In the 'no correlation' scenario the constraints barely change with smaller statistical uncertainties. Comparing the constraints from the data in Tab. I to the 300 fb^{-1} projection we find that the central values are slightly shifted and the 95 % intervals shrink minimally. For all coefficients we find agreement

with the SM within the 95 % intervals. In the 'best guess' scenario the picture changes: We find agreement with the SM for \tilde{C}_{tW} in the linear and quadratic implementation, where the 95 % interval shrinks by a factor of 1.2 while the central value is shifted to positive values. In the linear+ δ_{EFT} implementation small deviations of 2.5σ occur. The central value of \tilde{C}_{qq} decreases by a factor of 2 while the 95 % interval shrinks by a factor of 1.2, resulting in smaller deviation of around 2.5σ from the SM. In the case of $\tilde{C}_{\phi q}^{(3)}$ significant discrepancies occur. The 95 % interval reduces by a factor of 1.4, while the central value changes by a factor of up to 1.6. The deviation grow up to 9.0σ (linear), 8.9σ (quadratic) and 9.3σ (linear+ δ_{EFT}) so that new physics would be observed. In Fig. 6 we repeat the analysis from Fig. 2 for the 300 fb^{-1} projection. We find very similar results in all EFT-implementations. Increasing values of ρ_i lead to larger deviations from the SM. Similar to the fit to current data correlations of systematic uncertainties have a stronger impact on the constraints than correlations of theory uncertainties.

D. Comparison to literature

As a consistency check we compare our results to a recent global SMEFT analysis [7], which provides 95 % confidence level intervals from a fit to single top-quark production and top-quark decay data for the coefficients in Eq. (3). The dataset used in Ref. [7] is very similar to ours given in Tab. I, except for differential cross sections, not taken into account in Ref. [7]. To allow for a comparison of results we repeat our fits for the different fit models, linear, linear+ δ_{EFT} , and quadratic, defined in Sec. III in the 'no correlation' scenario to the data in Tab. I, excluding differential cross sections. Even though the smallest 95 % intervals in Bayesian statistics differ from confidence intervals in frequentist statistics, used in Ref. [7], we expect them to give very similar results.

Operators	95 % CL [7]	Linear	Linear+ δ_{EFT}	Quadratic
$\tilde{C}_{\phi q}^{(3)}$	[-0.29, 0.081]	[-0.30, 0.060]	[-0.24, 0.34]	[-0.31, 0.060]
\tilde{C}_{tW}	[-0.029, 0.029]	[-0.022, 0.012]	[-0.012, 0.014]	[-0.019, 0.014]
\tilde{C}_{qq}	[-0.031, 0.0069]	[-0.076, 0.064]	[-0.10, 0.13]	[-0.087, 0.077]

TABLE II: Marginalized 95 % confidence levels from Ref. [7] from a fit to single top-quark total cross sections and top-quark decay data together with the smallest 95 % intervals obtained in fits in the 'no correlation' scenario Eq. (7) to the data in Tab. I excluding differential cross sections. See text for details.

In Tab. II we give the 95 % confidence levels from Ref. [7] together with the smallest 95 % intervals obtained in our fits. The results are very similar for all three BSM coefficients in the three

different EFT-implementations. Small differences can be expected from the additional NLO QCD corrections to BSM contributions which are included in Ref. [7] and from inflated BSM contributions in our linear+ δ_{EFT} implementation.

IV. CONCLUSIONS

We studied the impact of correlations between (systematic and theory) uncertainties on multi-experiment, multi-observable analyses within SMEFT. Specifically, we performed a first quantitative study of such correlations entertaining the example of t -channel single top-quark production and top-quark decay. This data set allowed us to include 55 measurements from ATLAS, CMS, CDF and DO, given in Tab. I, in an analysis to constrain three Wilson coefficients (3). We considered different scenarios for theoretical and systematical uncertainties by varying two parameters ρ_{sys} and ρ_{th} in the correlation matrices based on simplifying assumptions. We highlighted two scenarios: The 'no correlation' scenario Eq. (7), which has been utilized in previous studies and the 'best guess' scenario Eq. (8), which incorporates additional correlations between measurements.

Not unexpectedly, correlations change the constraints on the Wilson coefficients significantly. Without correlations no deviations from the SM are found. In the case of strong correlations the SM prediction is not included anymore in the marginalized smallest 95% intervals of both $\tilde{C}_{\phi q}^{(3)}$ and \tilde{C}_{qq} , see Fig. 1. These deviations can be up to 4.5σ for $\tilde{C}_{\phi q}^{(3)}$ and 4.6σ for \tilde{C}_{qq} . On the other hand, different models (linear, quadratic, linear+ δ_{EFT}) for EFT-systematics from higher order corrections leave these findings – except for \tilde{C}_{qq} , where this can be expected – qualitatively untouched.

Correlations become even more crucial for future high-luminosity experiments where the importance of systematic and theory uncertainties is amplified. Assuming central values fixed, the SMEFT-fit leads to significant deviations from the SM at 9.0σ (linear), 8.9σ (quadratic) and 9.3σ (linear+ δ_{EFT}) in $\tilde{C}_{\phi q}^{(3)}$ in the 'best guess' scenario at 300 fb^{-1} , see Fig. 5. To benefit from improvements in statistics beyond 300 fb^{-1} requires improvements in experimental systematics and theoretical predictions.

Our analysis highlights the importance of correlations in global fits, especially for high-luminosity experiments. We suggest to consider different correlation scenarios and to take the corresponding variation into account when presenting results of global fits. At the same time, studies along the lines of Ref. [48] are encouraged to provide SMEFT-analyses with the requisite information about correlations of systematic and theory uncertainties. To conclude:

"Correlating uncertainties in global analyses within SMEFT matters in the future even more."

Acknowledgments

C.G. is supported by the doctoral scholarship program of the “Studienstiftung des Deutschen Volkes”.

-
- [1] S. Weinberg, *Phys. Rev. Lett.* **43**, 1566 (1979)
 - [2] W. Buchmüller and D. Wyler, *Nucl. Phys. B* **268**, 621 (1986). doi:10.1016/0550-3213(86)90262-2
 - [3] B. Grzadkowski, M. Iskrzynski, M. Misiak and J. Rosiek, *JHEP* **1010**, 085 (2010) doi:10.1007/JHEP10(2010)085 [arXiv:1008.4884 [hep-ph]].
 - [4] A. Cerri *et al.*, *CERN Yellow Rep. Monogr.* **7**, 867 (2019) doi:10.23731/CYRM-2019-007.867 [arXiv:1812.07638 [hep-ph]].
 - [5] N. P. Hartland *et al.*, *JHEP* **1904**, 100 (2019) doi:10.1007/JHEP04(2019)100 [arXiv:1901.05965 [hep-ph]].
 - [6] G. Durieux *et al.*, arXiv:1907.10619 [hep-ph].
 - [7] I. Brivio, S. Bruggisser, F. Maltoni, R. Moutafis, T. Plehn, E. Vryonidou, S. Westhoff and C. Zhang, arXiv:1910.03606 [hep-ph].
 - [8] S. Bickmann, J. Erdmann, C. Grunwald, G. Hiller and K. Kröninger, arXiv:1909.13632 [hep-ph].
 - [9] C. Degrande *et al.*, *JHEP* **1810**, 005 (2018) doi:10.1007/JHEP10(2018)005 [arXiv:1804.07773 [hep-ph]].
 - [10] M. Chala, J. Santiago and M. Spannowsky, *JHEP* **1904**, 014 (2019) doi:10.1007/JHEP04(2019)014 [arXiv:1809.09624 [hep-ph]].
 - [11] G. Durieux, F. Maltoni and C. Zhang, *Phys. Rev. D* **91**, no. 7, 074017 (2015) doi:10.1103/PhysRevD.91.074017 [arXiv:1412.7166 [hep-ph]].
 - [12] J. A. Aguilar-Saavedra, *Nucl. Phys. B* **843**, 638 (2011) Erratum: [*Nucl. Phys. B* **851**, 443 (2011)] doi:10.1016/j.nuclphysb.2011.06.003, 10.1016/j.nuclphysb.2010.10.015 [arXiv:1008.3562 [hep-ph]].
 - [13] J. D’Hondt *et al.*, *JHEP* **1811**, 131 (2018) doi:10.1007/JHEP11(2018)131 [arXiv:1807.02130 [hep-ph]].
 - [14] G. Durieux, J. Gu, E. Vryonidou and C. Zhang, *Chin. Phys. C* **42**, no. 12, 123107 (2018) doi:10.1088/1674-1137/42/12/123107 [arXiv:1809.03520 [hep-ph]].
 - [15] F. Maltoni, L. Mantani and K. Mimasu, *JHEP* **1910**, 004 (2019) doi:10.1007/JHEP10(2019)004 [arXiv:1904.05637 [hep-ph]].
 - [16] M. de Beurs, E. Laenen, M. Vreeswijk and E. Vryonidou, *Eur. Phys. J. C* **78**, no. 11, 919 (2018) doi:10.1140/epjc/s10052-018-6399-3 [arXiv:1807.03576 [hep-ph]].
 - [17] T. Neumann and Z. E. Sullivan, *JHEP* **1906**, 022 (2019) doi:10.1007/JHEP06(2019)022 [arXiv:1903.11023 [hep-ph]].
 - [18] A. Buckley *et al.*, *Phys. Rev. D* **92**, no. 9, 091501 (2015) doi:10.1103/PhysRevD.92.091501 [arXiv:1506.08845 [hep-ph]].

- [19] A. Buckley *et al.*, JHEP **1604**, 015 (2016) doi:10.1007/JHEP04(2016)015 [arXiv:1512.03360 [hep-ph]].
- [20] S. Brown *et al.*, PoS ICHEP **2018**, 293 (2019) doi:10.22323/1.340.0293 [arXiv:1901.03164 [hep-ph]].
- [21] J. A. Aguilar-Saavedra *et al.*, arXiv:1802.07237 [hep-ph].
- [22] J. Alwall *et al.*, JHEP **1407**, 079 (2014) doi:10.1007/JHEP07(2014)079 [arXiv:1405.0301 [hep-ph]].
- [23] T. Sjostrand, S. Mrenna and P. Z. Skands, JHEP **0605**, 026 (2006) doi:10.1088/1126-6708/2006/05/026 [hep-ph/0603175].
- [24] T. Sjostrand, S. Mrenna and P. Z. Skands, Comput. Phys. Commun. **178**, 852 (2008) doi:10.1016/j.cpc.2008.01.036 [arXiv:0710.3820 [hep-ph]].
- [25] A. D. Martin, W. J. Stirling, R. S. Thorne and G. Watt, Eur. Phys. J. C **63**, 189 (2009) doi:10.1140/epjc/s10052-009-1072-5 [arXiv:0901.0002 [hep-ph]].
- [26] G. Aad *et al.* [ATLAS Collaboration], Phys. Rev. D **90**, no. 11, 112006 (2014) doi:10.1103/PhysRevD.90.112006 [arXiv:1406.7844 [hep-ex]].
- [27] M. Aaboud *et al.* [ATLAS Collaboration], Eur. Phys. J. C **77**, no. 8, 531 (2017) doi:10.1140/epjc/s10052-017-5061-9 [arXiv:1702.02859 [hep-ex]].
- [28] CMS Collaboration [CMS Collaboration], CMS-PAS-TOP-14-004.
- [29] CMS Collaboration [CMS Collaboration], CMS-PAS-TOP-16-004.
- [30] H. L. Lai, M. Guzzi, J. Huston, Z. Li, P. M. Nadolsky, J. Pumplin and C.-P. Yuan, Phys. Rev. D **82**, 074024 (2010) doi:10.1103/PhysRevD.82.074024 [arXiv:1007.2241 [hep-ph]].
- [31] R. D. Ball *et al.* [NNPDF Collaboration], Nucl. Phys. B **877**, 290 (2013) doi:10.1016/j.nuclphysb.2013.10.010 [arXiv:1308.0598 [hep-ph]].
- [32] A. Czarnecki, J. G. Korner and J. H. Piclum, Phys. Rev. D **81**, 111503 (2010) doi:10.1103/PhysRevD.81.111503 [arXiv:1005.2625 [hep-ph]].
- [33] J. Gao, C. S. Li and H. X. Zhu, Phys. Rev. Lett. **110**, no. 4, 042001 (2013) doi:10.1103/PhysRevLett.110.042001 [arXiv:1210.2808 [hep-ph]].
- [34] N. Castro, J. Erdmann, C. Grunwald, K. Kröninger and N. A. Rosien, Eur. Phys. J. C **76**, no. 8, 432 (2016) doi:10.1140/epjc/s10052-016-4280-9 [arXiv:1605.05585 [hep-ex]].
- [35] M. Aaboud *et al.* [ATLAS Collaboration], JHEP **1704**, 086 (2017) doi:10.1007/JHEP04(2017)086 [arXiv:1609.03920 [hep-ex]].
- [36] M. Aaboud *et al.* [ATLAS Collaboration], Eur. Phys. J. C **78**, no. 2, 129 (2018) doi:10.1140/epjc/s10052-018-5595-5 [arXiv:1709.04207 [hep-ex]].
- [37] G. Aad *et al.* [ATLAS Collaboration], JHEP **1206**, 088 (2012) doi:10.1007/JHEP06(2012)088 [arXiv:1205.2484 [hep-ex]].
- [38] M. Aaboud *et al.* [ATLAS Collaboration], Eur. Phys. J. C **77**, no. 4, 264 (2017) doi:10.1140/epjc/s10052-017-4819-4 [arXiv:1612.02577 [hep-ex]].
- [39] S. Chatrchyan *et al.* [CMS Collaboration], JHEP **1212**, 035 (2012) doi:10.1007/JHEP12(2012)035 [arXiv:1209.4533 [hep-ex]].
- [40] V. Khachatryan *et al.* [CMS Collaboration], JHEP **1406**, 090 (2014) doi:10.1007/JHEP06(2014)090

- [arXiv:1403.7366 [hep-ex]].
- [41] A. M. Sirunyan *et al.* [CMS Collaboration], *Phys. Lett. B* **772**, 752 (2017) doi:10.1016/j.physletb.2017.07.047 [arXiv:1610.00678 [hep-ex]].
- [42] S. Chatrchyan *et al.* [CMS Collaboration], *JHEP* **1310**, 167 (2013) doi:10.1007/JHEP10(2013)167 [arXiv:1308.3879 [hep-ex]].
- [43] V. Khachatryan *et al.* [CMS Collaboration], *JHEP* **1501**, 053 (2015) doi:10.1007/JHEP01(2015)053 [arXiv:1410.1154 [hep-ex]].
- [44] V. Khachatryan *et al.* [CMS Collaboration], *Phys. Lett. B* **762**, 512 (2016) doi:10.1016/j.physletb.2016.10.007 [arXiv:1605.09047 [hep-ex]].
- [45] T. Aaltonen *et al.* [CDF Collaboration], *Phys. Rev. Lett.* **105**, 042002 (2010) doi:10.1103/PhysRevLett.105.042002 [arXiv:1003.0224 [hep-ex]].
- [46] T. Aaltonen *et al.* [CDF Collaboration], *Phys. Rev. D* **87**, no. 3, 031104 (2013) doi:10.1103/PhysRevD.87.031104 [arXiv:1211.4523 [hep-ex]].
- [47] V. M. Abazov *et al.* [D0 Collaboration], *Phys. Rev. D* **83**, 032009 (2011) doi:10.1103/PhysRevD.83.032009 [arXiv:1011.6549 [hep-ex]].
- [48] M. Aaboud *et al.* [ATLAS and CMS Collaborations], *JHEP* **1905**, 088 (2019) doi:10.1007/JHEP05(2019)088 [arXiv:1902.07158 [hep-ex]].
- [49] G. Apollinari, I. Béjar Alonso, O. Brüning, P. Fessia, M. Lamont, L. Rossi and L. Tavian, CERN Yellow Rep. Monogr. **4**, 1 (2017). doi:10.23731/CYRM-2017-004